Hindawi
International Journal of Aerospace Engineering
Volume 2022, Article ID 8435033, 18 pages
https://doi.org/10.1155/2022/8435033

Research Article

Enhancing Short-Term Prediction of BDS-3 Satellite Clock Bias Based with BSO Optimized BP Neural Network

Shaoshuai Ya,[1,2,3] **Xingwang Zhao**,[1,2,3] **Chao Liu**,[1,2,3] **Jian Chen**,[1,2,3] **Chunyang Liu**,[1,2,3] **and Haojie Hu**[1,2,3]

[1]*School of Spatial Informatics and Geomatics Engineering, Anhui University of Science and Technology, Huainan 232001, China*
[2]*Key Laboratory of Aviation-Aerospace-Ground Cooperative Monitoring and Early Warning of Coal Mining-Induced Disasters of Anhui Higher Education Institutes, Anhui University of Science and Technology, KLAHEI (KLAHEI18015), China*
[3]*Coal Industry Engineering Research Center of Mining Area Environmental and Disaster Cooperative Monitoring, Anhui University of Science and Technology, Huainan 232001, China*

Correspondence should be addressed to Xingwang Zhao; xwzhao@aust.edu.cn

Received 25 November 2021; Revised 1 March 2022; Accepted 15 March 2022; Published 11 May 2022

Academic Editor: Teng Wu

The satellite clock bias (SCB) prediction plays an important role in high-accuracy and real-time navigation and positioning. When predicting the SCB, the performance of the BP neural network is affected by the local optimum due to inaccurate initial parameters. Therefore, we propose an improved BP neural network based on the beetle swarm optimization (BSO-BP) algorithm to improve the performance of SCB prediction in third-generation Beidou satellite navigation system (BDS-3). The proposed model takes advantage of group learning strategy to optimize the initialization parameters of the BP neural network and obtains globally optimized parameters. In order to verify the proposed BSO-BP model, 15 BDS satellites are analyzed in terms of prediction accuracy and stability of SCB. The experimental results show that when predicting 1 hour SCB based on a 12 hours SCB data, the prediction accuracy of the BSO-BP model is the best, with an average accuracy of 0.064 ns. As compared with the LP, QP, and GM models, the average prediction accuracy of the proposed BSO-BP model increases by about 72.6%, 43.4%, and 86%, respectively. As the prediction time increases, the influence of the inaccurate initial parameters on SCB prediction gradually decreases, and the prediction accuracy improves. The proposed BSO-BP model has the best accuracy and stability when predicting the 1 h SCB based on the same data. The prediction stability of the proposed BSO-BP model improves by more than 36% as compared with LP, QP, and GM models. In addition, the prediction accuracies of PHM clock and Rb-II clock improved by more than 47%, as compared with that of the Rb clock. Therefore, the overall performance of the atomic clock based on BDS-3 is better than BDS-2. The positioning accuracy of the BSO-BP model can reach the centimeter level in east, north, and up directions.

1. Introduction

The position, navigation, and timing (PNT) service of global navigation satellite system (GNSS) is closely related to satellite clock bias (SCB) [1, 2]. The SCB as small as 1 ns produces a distance error of approximately 0.3 m, thus seriously influencing the positioning and timing accuracy of navigation systems [3, 4]. With the rapid development of GNSS technology, real-time clock bias prediction has become a research hotspot. Currently, there are two ways to obtain the real-time clock bias data, namely, IGS ultra-rapid ephemeris prediction products (IGU-P) and open real-time service (RTS). Both of these methods have different limitations, when used in GNSS applications. Though the IGU-P products satisfy the real-time requirements, their navigation and positioning precision are too low. On the other hand, the RTS provides real-time products with different requirements; however, it is inconvenient to obtain real-time clock bias products of Beidou navigation system (BDS). In addition, the RTS products developed by different agencies have different precisions, which seriously affect the results of high precision positioning [5]. Therefore, it is very

important to establish a high-precision SCB prediction model to achieve real-time high-precision SCB products for real-time positioning.

There are some commonly used SCB prediction models, including the linear polynomial (LP) model [6], the quadratic polynomial (QP) model [7], the grey model (GM) [8], the Kalman filter (KF) model [9], and the ARIMA time series model [10]. Please note that all of the aforementioned models are linear. However, the complex external environment results have a nonlinear effect on the SCB data. Consequently, a single linear model is unable to predict the SCB accurately. Few works proposed a linear combination model for predicting SCB, but the determination of the weight value is complex, and the tendency to improve the prediction accuracy is also limited [11].

With the advancements in machine learning, the neural networks have been introduced in the SBC prediction. The radial basis function neural network is used to predict the SCB of GPS for one day [12]. This method achieves a better accuracy than 1 ns, which verifies the feasibility of the model for performing SCB prediction. Wang et al. combine the advantages of fuzzy theory and neural network to predict the SCB of GPS [13]. The prediction results are 10 times better than the accuracies obtained by using IGU-P. When the wavelet function is used as an activation function in a neural network, it has a faster convergence speed and approximation ability, thus achieving highly accurate SCB prediction [14, 15]. It is noteworthy that the randomization of initial value of the wavelet neural network leads to the instability in prediction results. The genetic algorithm is utilized to optimize the initial value, which improves the accuracy and stability of SCB predictions [16, 17]. Zhao et al. used the grey neural network optimized by an intelligent algorithm to predict the clock bias and obtain better prediction accuracy of SCB as compared to the traditional models [18]. In addition, extreme learning machine optimized by particle swarm optimization algorithms improves the accuracy of International GNSS Monitoring and Assessment System (iGMAS) ultrafast SCB predictions by 50% approximately [19]. These works show that the neural networks have obvious advantages over the traditional models in SCB prediction.

The BP neural network was proposed in 1986 [20] and is used in various fields [21–25], due to its strong nonlinear learning ability. Zhu et al. used the BP neural network to predict the clock bias of the hydrogen (PHM) clock, which enhanced the prediction accuracy of PHM clock [26]. As the fitting residual has obvious nonlinear changes, the BP neural network is used to predict the fitting residuals of QP model with periodic item, which improves the accuracy of BDS ultrafast clock bias products [27]. In addition, the BP neural network optimized by the mind evolutionary algorithm is used to predict the GPS clock bias. The resulting prediction accuracy improves by more than 80% as compared with the QP model [28].

Due to strong global search abilities and fast search speed, the beetle swarm optimization (BSO) algorithm has been a focus of research community [29]. Parminder et al. use the BSO for heart disease detection and achieve accuracy and precision of 99.1% and 99.37%, respectively [30]. In the field of intelligent robotics, BSO is used for planning the trajectory of robots, which has a faster calculation speed and better control performance than the existing algorithms [31]. Moreover, the BSO is used to plan the three-dimensional path, which is about 90% of the PSO path planning length [32]. The BP neural network is easily trapped in a local optimum. The BSO algorithm is used to optimize the initial value parameters. In this work, in order to improve the accuracy and stability of clock bias prediction, the BSO-BP model is introduced for short-term clock bias prediction.

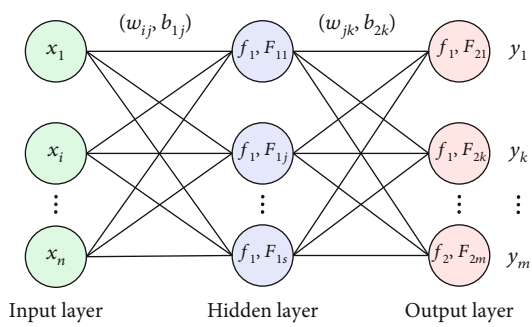

Figure 1: The architecture of BP neural network.

The rest of the manuscript is organized as follows. In Section 2, we present some basic principles about the BSO-BP model. In Section 3, preprocessing of clock bias data, prediction accuracy, and stability of gray system model (GM (1,1)), quadratic polynomial (QP) model, linear polynomial (LP), and BSO-BP model are compared and analyzed. In Section 4, PPP validation with predicted clock. Finally, in Section 5, we conclude this work.

2. An Improved BDS Clock Offset Prediction Mode

In the section, for a clear understanding of the improved model for SCB prediction, the basic principles of BP neural network and BSO algorithm are introduced first. Then, the flow of BSO-BP model is given in details.

2.1. BP Neural Network. The BP neural network is based on error back propagation and is mainly divided into two processes, including forward propagation and back propagation of error [33, 34]. During the process of back propagation, the weights and thresholds of the network are updated based on the feedback error, such that the actual output value of the network is closer to the expected output value.

As presented in Figure 1, the architecture of BP neural network comprises an input layer, an output layer, and a hidden layer. x_i denotes the input of the network, and w_{ij} and b_{1j} denote the weights and thresholds for the input to hidden layer, respectively. The excitation function of the hidden layer is f_1, output value of the hidden layer is F_{1j}, and weight and threshold for the hidden layer to the output layer are expressed as w_{jk} and b_{2k}, respectively. Similarly, the

excitation function of output layer is f_1, output value obtained from the output layer is F_{2k}, and y_k denotes the true value.

We normalize the input of the network as follows:

$$\begin{cases} X_i = \dfrac{x_i - \min\{x_i\}}{\max\{x_i\} - \min\{x_i\}}, \\ Y_m = \dfrac{y_m - \min\{y_m\}}{\max\{y_m\} - \min\{y_m\}}. \end{cases} \tag{1}$$

Based on the weights, thresholds, and excitation function from the input to the hidden layer and, the output value is computed as follows:

$$F_{1j} = f_1\left(\sum_{i=1}^{n} w_{ij} \cdot X_i + b_{1j}\right), \tag{2}$$

where n denotes the number of neurons in the hidden layer. Similarly, based on the weights, thresholds, and excitation function from the hidden to the output layer and F_{1j}, the output is computed as follows:

$$F_{2k} = f_2\left(\sum_{j=1}^{n} w_{jk} \cdot F_{1j} + b_{2k}\right). \tag{3}$$

The error between the actual value and the estimated value is computed as follows:

$$E = \frac{1}{2}\sum_{k=1}^{m} (y_k - F_{2k})^2, \tag{4}$$

where m denotes the number of training samples. Based on this error, the weight and bias terms are updated by using the gradient descent method as follows:

$$\begin{cases} w' = w - \Delta w, \Delta w = -\eta \dfrac{\partial E'}{\partial w}, \\ b' = b - \Delta b, \Delta b = -\eta \dfrac{\partial E'}{\partial b}, \end{cases} \tag{5}$$

where E' denotes the error for each layer of the neural network, η denotes the learning rate, w' denotes the corrected weight, and b' denotes the corrected threshold.

Considering the SCB data of BDS, the number of neurons in the input layer and the output layer of the BP neural network is both 1. Therefore, the number of neurons $l = \sqrt{p+q} + a'$, where p denotes the number of neurons in the input layer, q denotes the number of neurons in the output layer, and a' is usually between 1 and 10.

The BP neural network has superior nonlinear mapping and adaptive learning abilities. Therefore, it is more efficient than the conventional models in dealing with the nonlinear problems. However, the precision and convergence speed of the BP neural network depend on the initial weights and thresholds. The random generation of these parameters may trap the network in a local minimum. In order to solve this aforementioned issue, the BSO algorithm is introduced to optimize the initial parameters and improve the training results of the BP neural network.

2.2. Beetle Swarm Optimization (BSO) Algorithm. The BSO algorithm is an intelligent optimization algorithm that uses the fitness function value of two tentacle angles of each bull in the bull group to seek the optimal position of the bull group. This algorithm has the advantage of individual evolution and group learning. When searching for the optimal solution, the optimal fitness value of the current individual is recorded. Then, the information interaction with the whole group is performed to determine the optimal fitness value of the group. Finally, the position and speed of the beetle swarm are updated by combining the group and individual optimization [35–37].

When using the BSO algorithm for optimization, we use a random function to initialize the position and speed of the beetle swarm:

$$\begin{cases} X = \text{rands}(D, m), \\ V = \text{rands}(D, m), \end{cases} \tag{6}$$

where D denotes the number of parameters, m denotes the number of beetles, $X = (X^1, X^2, \cdots X^m)$ represents the initial position of the beetle swarm, $X^i = (x_1^i, x_2^i, \cdots x_D^i)$ represents the position of i-th beetle, $V = (V^1, V^2, \cdots V^m)$ represents the initial speed of the beetle swarm, and $V^i = (v_1^i, v_2^i, \cdots v_D^i)$ denotes the speed of i-th beetle. Please note that the fitness of each beetle is calculated based on the initialization parameters and fitness function and by recording the optimal value f_g for each beetle and optimal value f_b of beetle swarm. The updated V is mathematically expressed as follows:

$$V_{t+1} = V_t \cdot w + c1 \cdot r1 \cdot \left(X - f_g\right) + c2 \cdot r2 \cdot (X - f_b), \tag{7}$$

where V_t and V_{t+1} denote speed of the t-th and $t+1$-th iteration, respectively, w denotes the inertia weight, $c1$ and $c2$ represent the learning factors, and $r1$ and $r2$ represent the random numbers between 0 and 1. In order to enable the algorithm to avoid the local optimum, the value of V is constrained between $v_{\min}$ and $v_{\max}$. Please note that the inertia weight is generally a linear variable.

$$w_i = w_{\max} - (w_{\max} - w_{\min}) \cdot \left(\frac{i}{n}\right), \tag{8}$$

where $w_{\max}$ and $w_{\min}$ denote the maximum and minimum inertia weight and n denotes the maximum number of iterations. For t-th iteration, the mathematical expressions for the left and right tentacles of the beetle are

$$\begin{cases} X_l^i = X^i - V^i \cdot d_0/2 \\ X_r^i = X^i + V^i \cdot d_0/2 \end{cases}, d_0 = \frac{\text{step}}{c}, \tag{9}$$

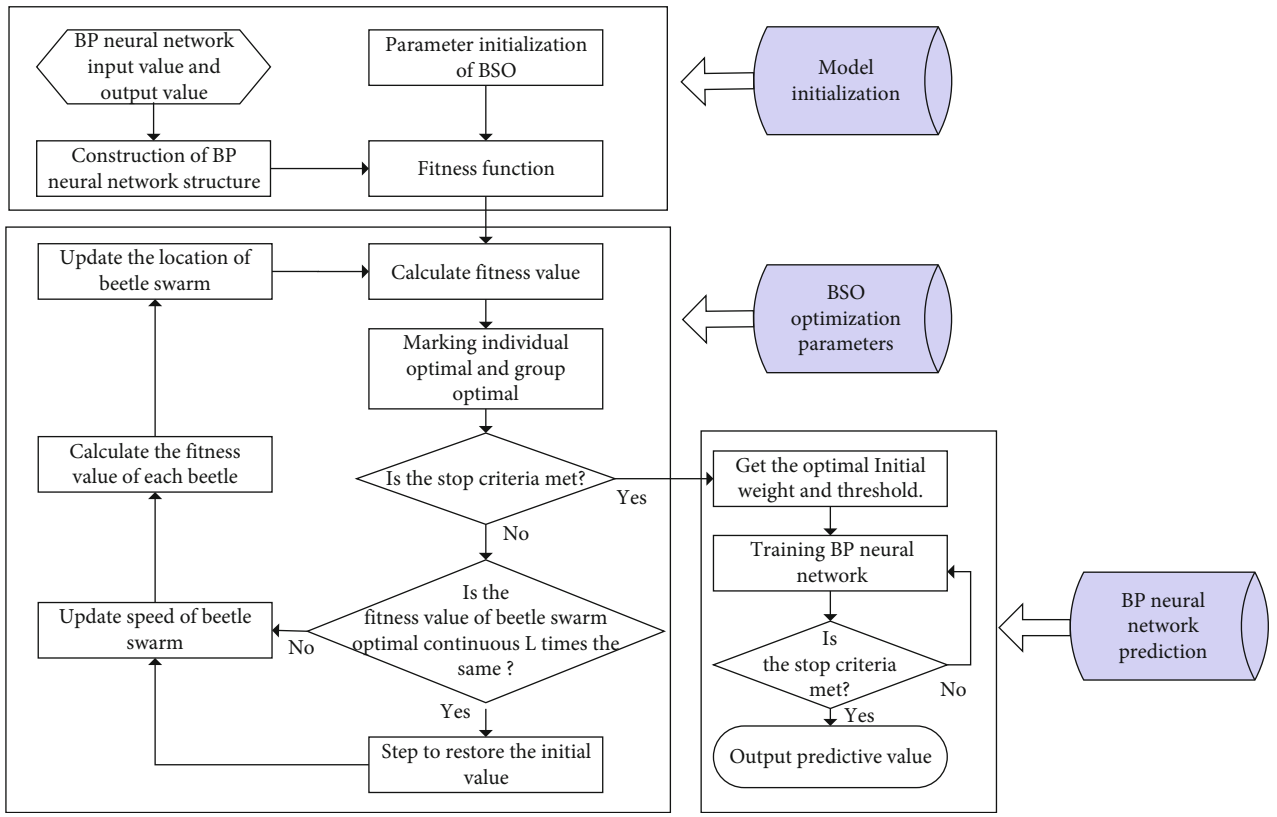

Figure 2: The workflow of the proposed BSO-BP algorithm.

Table 1: Types of BDS satellite clocks used in this work.

Satellite	Clock type	PRN
BDS-2	Rb	C01, C03, C04, C05, C14
BDS-3	Rb-II	C20, C22, C23, C24, C32
	PHM	C26, C27, C28, C29, C34

where X_l^i and X_r^i represent the positions of left and right tentacles of the beetle, c denotes the ratio of step length of tentacles, and d_0^t denotes the distance between the left tentacle and right tentacle. The update expression of the position of beetle swarm is

$$\begin{cases} X_{t+1}^i = X_t^i + \lambda \cdot V_t^i + (1\text{-}\lambda) \cdot \xi_t^i, \\ \xi_t^i = \text{step}_t \cdot V_t^i \cdot \text{sign}\left(f\left(X_r^i\right) - f\left(X_l^i\right)\right), \end{cases} \tag{10}$$

where λ denotes a positive constant and ξ_t^i represents the change in beetle position. The step is updated in a decreasing manner as follows:

$$\text{step}_{t+1} = \text{step}_t \cdot eta, \tag{11}$$

where *eta* represents the updating factor of the step. Based on (6)–(11), the position and speed of the beetle swarm are constantly updated until the iterative process is terminated. The optimal positions of the beetle swarm are used as the initial parameters of the BP neural network.

2.3. Beetle Swarm Optimization BP Neural Network (PSO-BP) Model Used for SCB Prediction. The BP neural network makes the output value of the network approach the true value by continuously correcting the weights and thresholds. However, the initial weights and threshold of the BP neural network are selected randomly, which leads to a nonoptimal solution. In this work, we use the BSO algorithm to optimize the BP neural network for predicting the SCB. The main process is divided into two parts: (1) The BSO algorithm optimizes the initial parameters of the network. (2) The optimal initial values estimated by the BSO are substituted in the BP neural network for training. The major steps of the algorithm are shown in Figure 2.

Step 1. The number of hidden layer nodes in the BP neural network is determined based on the input and output values of the network, and the parameters of the BSO algorithm are initialized.

Step 2. The fitness function is used to calculate the fitness value of each beetle, and the individual optimal and group optimal are marked.

Step 3. Determine if the BSO algorithm satisfies the termination conditions. If the termination conditions are satisfied, go to Step 6. Otherwise, go to Step 4.

Step 4. In order to enhance the searching ability of the algorithm, a condition is added to the algorithm to determine if the value of optimal fitness function is same for L consecutive iterations. As the step size of the algorithm is progressively updated, the late step size is small, which is not conducive to global search. Therefore, when the value of optimal fitness function is same for L consecutive times, the step size is restored to the initial value.

Step 5. Update the speed and position of the beetle swarm using expressions (6)–(11).

Step 6. The optimal parameters obtained by the BSO algorithm are substituted in the BP neural network for continuous training and prediction.

3. Experimental Results and Analysis

In this work, we use the final clock products for one week (DOY 163-169, 2020) from WHU (Wuhan University). The sampling interval is 30 s. 15 satellites used for experiments are shown in Table 1, which include five rubidium (Rb) clocks, five new rubidium (Rb-II) clocks, and five hydrogen (PHM) clocks. The mean absolute deviation (MAD) is used in data preprocessing to detect the outliers in SCB data. In addition, we interpolate distorted data by linear method. Then, the model is established by using the preprocessed SCB data. Finally, the precise SCB data corresponding to the prediction period is selected as the reference data. The root mean square error (RMS) [38] and standard deviation (STD) are used as the accuracy metrics to evaluate the proposed model. In this work, six tests are performed to analyze the accuracy and stability of the proposed BSO-BP model. In Sections 3.1-3.5, we use the day (DOY 163, 2020) of SCB data to analyze. In Section 3.1, the MAD method is used to preprocess the SCB data. In Section 3.2, the frequency and phase data to perform predictions and analyze their prediction accuracies. In Section 3.3, we analyze the prediction performance of BP and the proposed BSO-BP models. In Section 3.4, 15 satellites were used to analyze the prediction accuracies of the proposed BSO-BP model with different fitting time and different prediction time. In Section 3.5, the prediction stability of different models and atomic clocks is analyzed. In Section 3.6, we use 6 consecutive days (DOY 164-169, 2020) of SCB data for accuracy and stability analysis.

3.1. Data Preprocessing. It is notable that the phase data of SCB has obvious trends and large values, which make it difficult to effectively detect the outliers using the original SCB data. Moreover, the BP neural network effectively adapts to nonlinear data. Therefore, it is necessary to convert the original SCB data into frequency data by using the following expression:

$$y_i = \frac{x_{i+1} - x_i}{\tau}, \tag{12}$$

where x_i represents the SCB sequence, τ denotes the sampling interval of SCB, y_i represents the frequency data, n represents the total number of epochs for a sequence, and $i = 1, 2, 3, \cdots, n-1$. In order to evaluate the prediction accuracy and facilitate the user's application, the frequency data is reduced to the SCB data by using as follows:

$$x_j = x_l + \tau \cdot \sum_{j=1}^{g} y_j, \tag{13}$$

where x_l denotes the last SCB data used for training the BP neural network, y_j denotes the predicted frequency data, and x_j denotes the predicted SCB data. When detecting the gross error of the clock bias, the MAD method is generally used consisting of following steps.

Step 1. Convert the SCB data to frequency data using (12).

Step 2. Arrange the frequency data from small to large and compute the median (m) of the sequence.

Step 3. Calculate the value of MAD based on m, $\text{MAD} = \text{median}\{|y_i - m|/0.6745\}$.

Step 4. The value of k times MAD is used as the threshold for detecting the outliers, and the y_i exceeding the threshold is marked as outliers. Generally, k is between 3 and 5. In this work, $k = 3$.

Step 5. If the i-th frequency is marked as an outlier, the SCB of the $i+1$-th epoch is eliminated, and the SCB of the epoch is restored by linear interpolation.

As presented in Figure 3, there are many gross errors in the original frequency data. After preprocessing the data using MAD, the gross errors are effectively eliminated. The values of frequency data are between 0.55 and 0.75 (10-11 Hz), so its fluctuations are more stable. In addition, the value of phase data is large and does not change significantly after preprocessing. Therefore, the frequency data is more suitable for gross error detection of SCB data.

3.2. Comparative Analysis of Phase and Frequency Data. The SCB data of C01 (Rb clock), C23 (Rb-II), and C34 (PHM clock) are selected to analyze that the BP neural network has better adaptability to frequency data. We use the phase and frequency data obtained during the first 12 hours of the day for predicting the SCB value of the next 10 min (20 epochs) using the BP network. The predicted SCB value for 30 consecutive times is recorded, and the RMS value is used as the metric to evaluate the prediction result.

As presented in Figure 4, the RMS of 30 consecutive SCB values predicted using phase data of C01, C23, and C34 are larger than using the frequency data. Therefore, when the BP neural network is used for clock bias prediction, the prediction accuracy for frequency data of Rb clock, Rb-II clock, and PHM clock improves by different degrees as compared with the phase data. In addition, the variations in the RMS values of the three satellites show that when the frequency data is used to predict, the prediction accuracy of the three

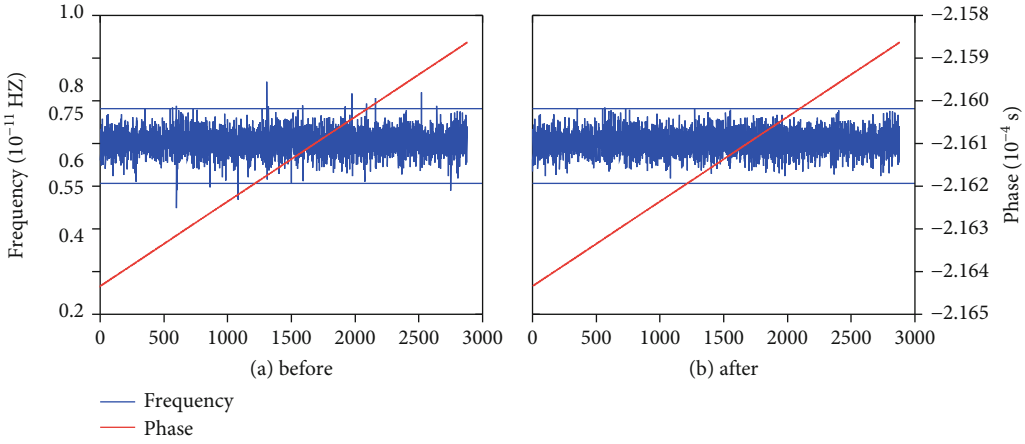

Figure 3: The gross error detection results of C28 SCB data: (a) the original data; (b) the data preprocessed by MAD.

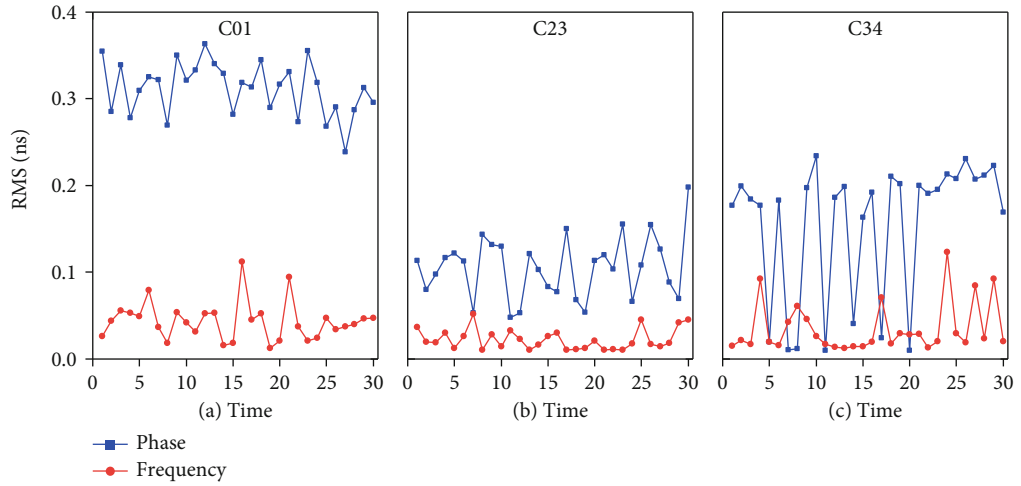

Figure 4: (a) The RMS value of 30 C01 continuous predictions. (b) The RMS value of 30 C23 continuous predictions. (c) The RMS value of 30 C34 continuous predictions. The red color denotes the results predicted using the phase data, and the blue represents the results predicted using the frequency data.

satellites is generally within 0.1 ns, while the prediction accuracy of the phase data is within 0.4 ns. Therefore, the variations in prediction accuracy of phase data for 30 consecutive times are larger, especially for C34, i.e., 0.23 ns. Contrary, the prediction accuracy for frequency data is about 0.13 ns. Therefore, the BP neural network using the frequency data for SCB prediction significantly improves the performance of predictions.

3.3. Comparative Analysis of BS0-BP and BP. The section selects three different types of atomic clocks C01, C23, and C34 as discussed in the aforementioned experiments to verify the prediction performance of the improved BSO-BP model. We use the data obtained during the first 12 hours of the day to fit the clock error half an hour after the prediction. The BP and proposed BSO-BP models are used to predict the clock errors for 10 consecutive times, and RMS values are recorded. The changes in the RMS values predicted by the BP and BSO-BP models are compared and analyzed.

As presented in Figure 5, the RMS value of BSO-BP model is significantly smaller than that of the BP model. In addition, the RMS values of the proposed BSO-BP for 10 consecutive times are relatively stable. In addition, for C01, C23, and C34 satellites, the prediction accuracy of BSO-BP model improves by 69.5%, 80.8%, and 86.7%, respectively, as compared with the BP model. The minimum RMS value predicted by the BSO-BP model is better than that of the BP model. As the weights and thresholds of the BP neural network are not optimal, its prediction accuracy is low, and the RMS value changes significantly. The BP neural network optimized using the BSO enhances the global optimization ability of the BP neural network and improves its prediction accuracy.

3.4. Accuracy Analysis of Predicted SCB. In order to analyze the prediction accuracy of the proposed BSO-BP model, Rb (C01, C03, C04, C04, C14) of BDS-2, Rb-II (C20, C22, C23, C24, C32), and PHM (C26, C27, C28, C29, C34) clocks of BDS-3 are selected to perform experiments. The

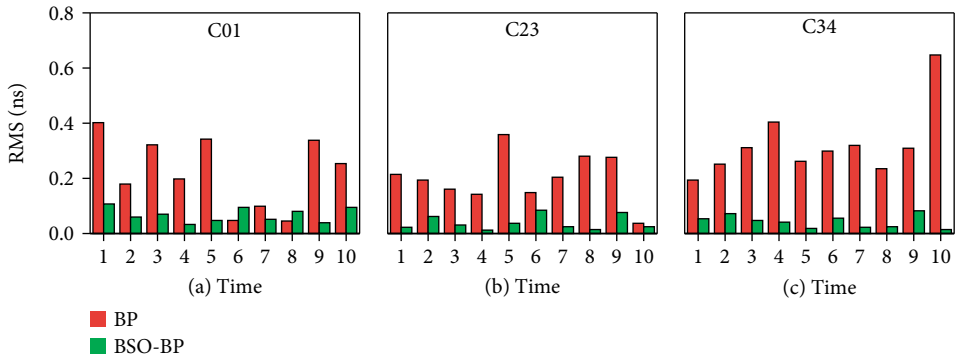

Figure 5: (a) The RMS value of 10 C01 continuous predictions. (b) The RMS value of 10 C23 continuous predictions. (c) The RMS value of 10 C34 continuous predictions. The green color represents the results predicted using the proposed BSO-BP model, and the red color represents the results predicted using the BP model.

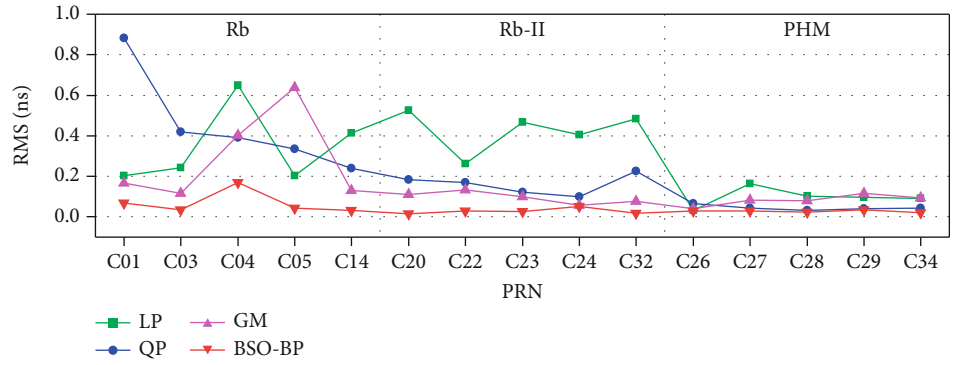

Figure 6: The prediction accuracy of 15 BDS satellites for 0.5 hours using 6 hours SCB data.

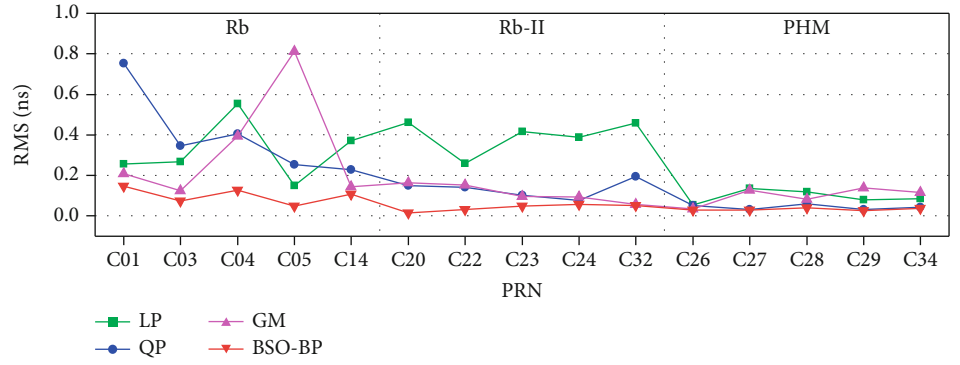

Figure 7: The prediction accuracy of 15 BDS satellites for 1 hour using 6 hours SCB data.

experimental process is as follows: (1) The SCB data of the first 6 hours of the day is used to predict the clock bias of next 0.5 and 1 hour. (2) The SCB data of the first 12 hours of the day is used to predict the clock bias of next 0.5 and 1 hour. The RMS values of prediction accuracies obtained for different schemes are counted, and the accuracy analysis of different fitting time and different prediction time is performed by using the LP, QP, GM, and BSO-BP models.

As presented in Figure 6, among the four models, the prediction accuracies of LP, QP, and GM are poor. In addition, the RMS of the predicted values for different satellites change significantly. The results show that the prediction RMS values of the LP model for C04 and C26 are about 0.6 ns and 0.1 ns, respectively, the prediction RMS values of the QP model for C01 and C28 are about 0.8 ns and 0.1 ns, respectively, and the prediction RMS values of the GM model for C05 and C28 are about 0.8 ns and 0.1 ns, respectively. Therefore, the variation in prediction accuracies is at least 0.5 ns. Contrary, the RMS values of SCB prediction obtained using the proposed BSO-BP model are all within 0.2 ns. Moreover, the variation in accuracies is better as compared to other methods.

At the same time, as presented in Figure 7, the BSO-BP model maintains high prediction accuracy with an increase

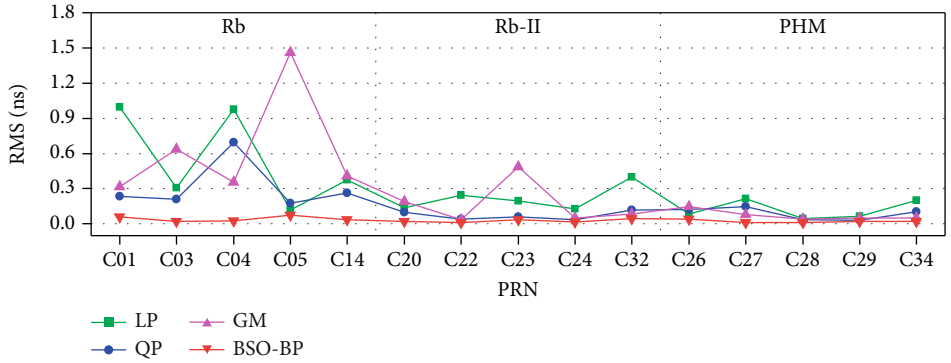

Figure 8: The prediction accuracy of 15 BDS satellites for 0.5 hours using 12 hours SCB data.

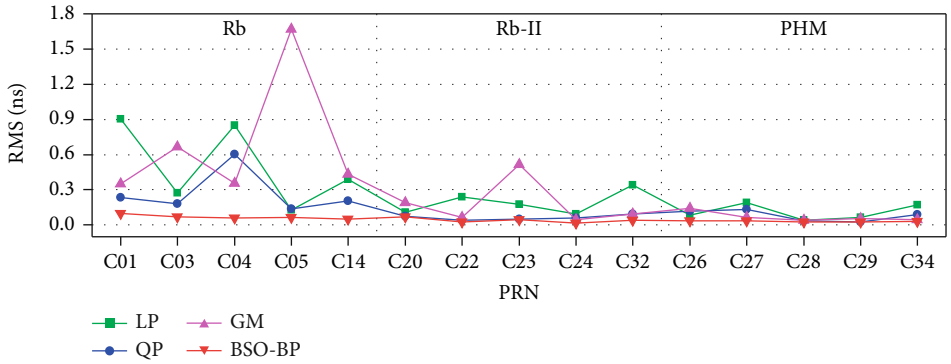

Figure 9: The prediction accuracies of 15 BDS satellites for 1 hour using 12 hours SCB data.

in the prediction time. On the other hand, the accuracies of other models do not change significantly. It is noteworthy that when the four models have different prediction time, the best prediction accuracy is for the PHM clock, followed by the Rb-II clock, and the Rb clock. This is related to the physical characteristics of different atomic clocks and does not change with the increase in prediction time.

As presented in Figure 8, with an increase in fitting time, the prediction accuracy of the BSO-BP model remains optimal. Please note that this accuracy is slightly better than the accuracy obtained for 0.5 hours based on the data of 6 hours. In addition, with an increase in fitting time, the changes in accuracies for the LP, QP, and GM models for different satellites are also different. The results show that the prediction accuracy of the LP model for C01 decreases with an increase in the fitting time, while the prediction accuracy for C20 is significantly improved. Similarly, the QP and GM models also depict the same phenomenon. As presented in Figure 9, with an increase in the forecast time, the results are similar to those presented in Figures 6 and 7.

The prediction residuals reflect the accuracy of the predicted value. The farther the residual is from 0, the worse is the prediction accuracy and vice versa. Therefore, the prediction residuals of C01 (Rb clock), C23 (Rb-II clock), and C27 (PHM clock) satellites are selected to perform analysis, as shown in Figures 10 and 11.

It is evident from Figures 10 and 11 that when the fitting time is 6 hours and the prediction time is 1 hour, the prediction residuals of the BSO-BP model for the SCB of three satellites fluctuate around 0, which is the closest to the true value of SCB. However, the LP, QP, and GM models are affected differently for different satellites, and the degree of deviation from the true value varies significantly. For instance, the prediction residuals of QP model for C01 deviate from the true value critically, and the prediction residuals of C23 and C27 are similar to the BSO-BP model, i.e., close to the true value. The degree of deviation in cases of LP and GM models is obviously larger than that of the BSO-BP model. The results show that by increasing the fitting time, the prediction residual of the BSO-BP model is still near 0, while the prediction residuals of the LP, QP, and GM models are not stable. The deviation of the prediction residual in case of LP model for C01 is larger as compared to C23. The deviation in the predicted residual from the true value is smallest in case of the BSO-BP model. Moreover, the predicted residuals for the proposed model do not vary by changing the fitting time.

Based on the aforementioned analysis, the prediction accuracy of the proposed BSO-BP model is the best. In order to further analyze the prediction accuracy of the aforementioned models, the average prediction accuracy of different atomic clocks is calculated, as shown in Tables 2 and 3.

It is evident from Tables 2 and 3 that when the fitting time is 6 hours, the prediction accuracy of the proposed BSO-BP model for PHM clock and Rb-II clock is within 0.05 ns, and the prediction accuracy for Rb clock is also approximately 0.1 ns, which is much better as compared to the other models. The analysis of prediction accuracy for

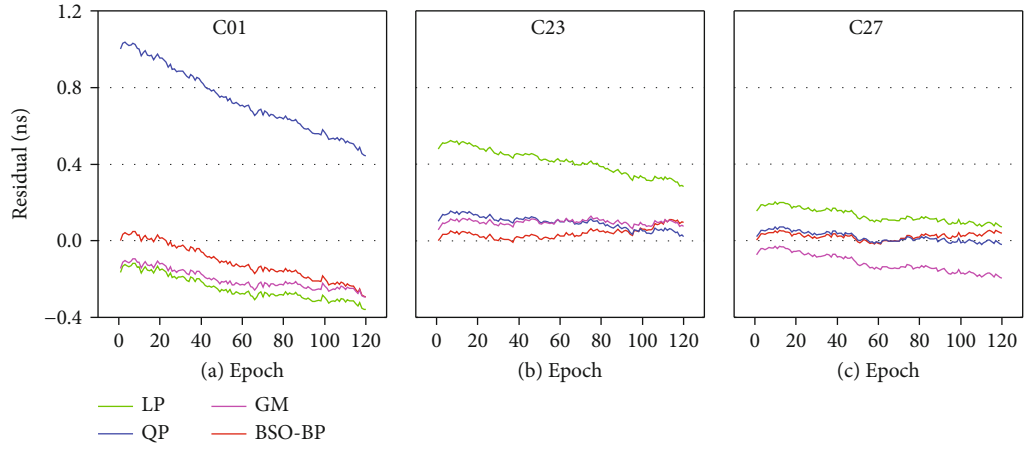

Figure 10: The residual plot of three satellites using 6 hours data to forecast 1 hour: (a) the residual value of C01 forecast 1 hour; (b) the residual value of C23 forecast 1 hour; (c) the residual value of C27 forecast 1 hour.

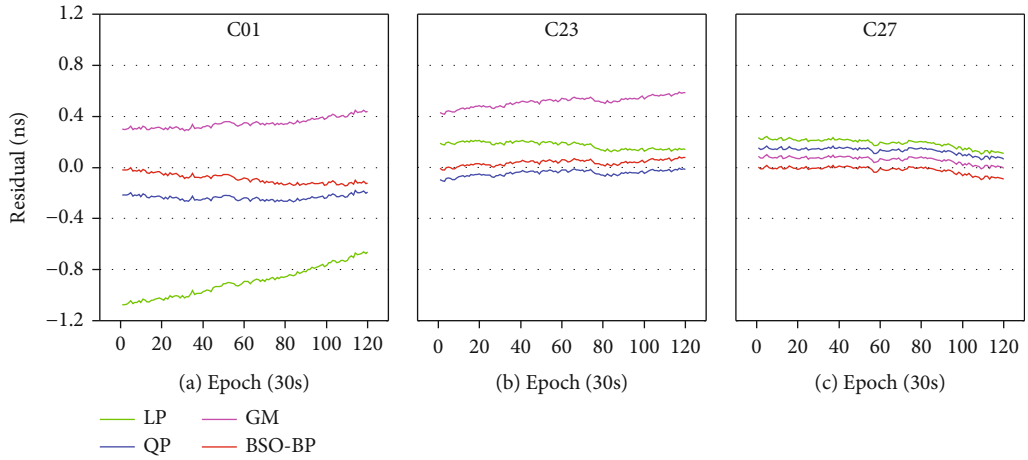

Figure 11: The residual plot of three satellites using 12 hours data to forecast 1 hour: (a) the residual value of C01 forecast 1 hour; (b) the residual value of C23 forecast 1 hour; (c) the residual value of C27 forecast 1 hour.

Table 2: The average prediction accuracy for 0.5 hours and 1 hour for three different types of clocks based on 6-hour SCB data.

Clock type	0.5 h					1 h				
	LP	QP	GM	BSO-BP	Mean	LP	QP	GM	BSO-BP	Mean
Rb	0.342	0.453	0.291	0.070	0.289	0.319	0.398	0.336	0.101	0.289
Rb-II	0.429	0.160	0.095	0.028	0.178	0.397	0.133	0.113	0.041	0.171
PHM	0.096	0.045	0.082	0.028	0.063	0.094	0.044	0.100	0.033	0.068
Mean	0.289	0.220	0.156	0.042		0.270	0.191	0.183	0.058	

Table 3: The average prediction accuracy for 0.5 hours and 1 hour for three different types of clocks based on 12-hour SCB data.

Clock type	0.5 h					1 h				
	LP	QP	GM	BSO-BP	Mean	LP	QP	GM	BSO-BP	Mean
Rb	0.554	0.317	0.636	0.043	0.387	0.508	0.273	0.694	0.068	0.386
Rb-II	0.221	0.070	0.170	0.026	0.122	0.192	0.064	0.181	0.040	0.119
PHM	0.122	0.089	0.073	0.022	0.076	0.111	0.081	0.070	0.031	0.073
Mean	0.299	0.158	0.293	0.030		0.270	0.139	0.315	0.046	

different prediction times under the same fitting time shows that when 6-hour SCB data is used, the prediction accuracies of the GM and BSO-BP models decrease by increasing the prediction time. The prediction accuracies of the LP and QP models increase with an increase in prediction time. This is caused by the trend of prediction residual and the initial prediction residual. For instance, the initial residual of the QP model in Figure 9(a) is about 1 ns. With an increase in prediction time, the prediction residual decreases, and the prediction clock difference constantly approaches the true value. Therefore, the prediction accuracy increases. Similarly, in Figure 9(b), the LP model depicts the same trend. These trends are also similar in the case of using 12 hours for fitting to predict 0.5 h and 1 h.

Based on the analysis of prediction accuracies obtained for the same prediction time under different fitting time shows that when fitting 6 hours and 12 hours to forecast 0.5 hours, respectively, for the Rb clock, the prediction accuracies of the LP and GM models decrease with an increase in the fitting time, while the prediction accuracies of the QP and BSO-BP models increase with an increase in the fitting time. For the Rb-II clock, the prediction accuracies of the LP, QP, and BSO-BP models increase with an increase in the fitting time, while the GM model shows an opposite trend. For PHM clocks, the accuracies of the LP and QP models decrease with an increase in fitting time, while the GM and BSO-BP models improve constantly. The results show that the LP, QP, and GM models have different variations under the influence of different atomic clocks, while the proposed BSO-BP model is relatively stable under different types of atomic clocks. In addition, the prediction accuracy of the proposed model increases with an increase in fitting time.

It is evident from the prediction mean values of different models that the prediction accuracy of BSO-BP model improves by varying degrees as compared with other models. For instance, when fitting 6 hours to predict the next 0.5 hours and 1 hour clock bias, the prediction accuracy of the BSO-BP model improves by about 85.5%, 81%, and 73.1% and 78.5%, 58.3%, and 68.3% as compared with the LP, QP, and GM models, respectively. When the fitting time changes, the prediction accuracy of the proposed BSO-BP model is still better than the other three models. It is evident from the prediction mean values of different atomic clocks that the prediction accuracies of PHM clock and Rb-II clock increase by about 80.4% and 68.5%, respectively, as compared with that of the Rb clock, and do not change with the change in fitting time and prediction time. In addition, when the fitting time is the same, the prediction accuracies of the three atomic clocks for 0.5 hours and 1 hour are almost unchanged. Therefore, the prediction accuracies of different atomic clocks do not improve significantly with an increase in fitting time.

3.5. Stability Analysis of Predicted SCB. The section selects 15 satellite atomic clocks as discussed in the aforementioned experiments to evaluate the prediction stability of the proposed model. Moreover, the experiment increases a lot of data to improve the accuracy and reliability of analysis. We use five groups of clock bias data, i.e., 1-6, 2-7, 3-8, 4-9, and 5-10 hours, of a day to predict the clock bias of next 1 hour. The residual values of the five groups of prediction data are counted, and the prediction STD of the LP, QP, GM, and BSO-BP models by fitting 6 hours are calculated. In this work, since the STD reflects the degree of deviation of data, it is considered to be a metric to evaluate the stability. In addition, in order to analyze the influence of different fitting times on the prediction stability, five groups of clock bias data of 1-12, 2-13, 3-14, 4-15, and 5-16 hours of a day are used to predict the next 1-hour clock bias. The STD of the four models fitting 12-hour clock bias is compared with the STD of fitting 6-hour clock bias.

As shown in Figure 12, the shorter the length of the box, the more concentrated is the data and more stable is the prediction model. It is evident from Figure 12(a) that the residual value of BSO-BP model is more concentrated, and the prediction results are more stable as compared to other models. The residual values of the BSO model fluctuate around 0, and the residual values of other models vary significantly. For instance, the prediction stability of the GM model for CO3 is better than that of the BSO-BP model. However, for other satellites, the prediction stability of the GM model is much worse than the proposed BSO-BP model. The prediction stabilities of the QP and LP models also vary significantly for different satellites. Similar conclusions can be drawn between Figures 12(b) and 12(c).

In addition, for the Rb and Rb-II clocks, the prediction residuals obtained by using the LP model are far from 0, so the prediction SCB of the LP model deviates from the true value critically. For PHM clocks, the prediction SCB of the GM model largely deviates from the true value, and the residual value is dispersed, leading to poor prediction stability. The stability of the QP model for different atomic clocks also changes substantially. Therefore, the prediction stability of the model is influenced by the type of atomic clock.

The box plots of different atomic clocks show that the residual value of Rb clock changes between the range of -1.5 ns and 1 ns, the residual value of Rb-II clock changes between the range of -0.4 ns and -0.8 ns, and the residual value of PHM clock changes between the range of -0.3 ns and 0.4 ns. Therefore, the stability of PHM clock is better as compared to Rb-II and Rb clocks.

It is evident from Figure 13 that with an increase in fitting time, the prediction results of different models change differently. For Rb-II clock, the distance between the prediction residual of the LP model and 0 is very smaller, and the change in the prediction residual of the QP model is not obvious, while the degree of concentration of the prediction residual values of the GM model and the degree of deviation from 0 are better. The prediction stability of the BSO-BP model shows small changes and the best prediction stability.

It is evident from Table 4 that the prediction STD of the proposed BSO-BP model for different types of atomic clocks is the smallest. When we use the SCB data of 6 hours for predicting the clock bias of next 1 hour, the prediction stability of the BSO-BP model improves by approximately 50%, 50%, and 56.5% as compared with the LP, QP, and GM models, respectively. With an increase in the fitting time, the prediction stabilities of the LP, GM, and BSO-BP models

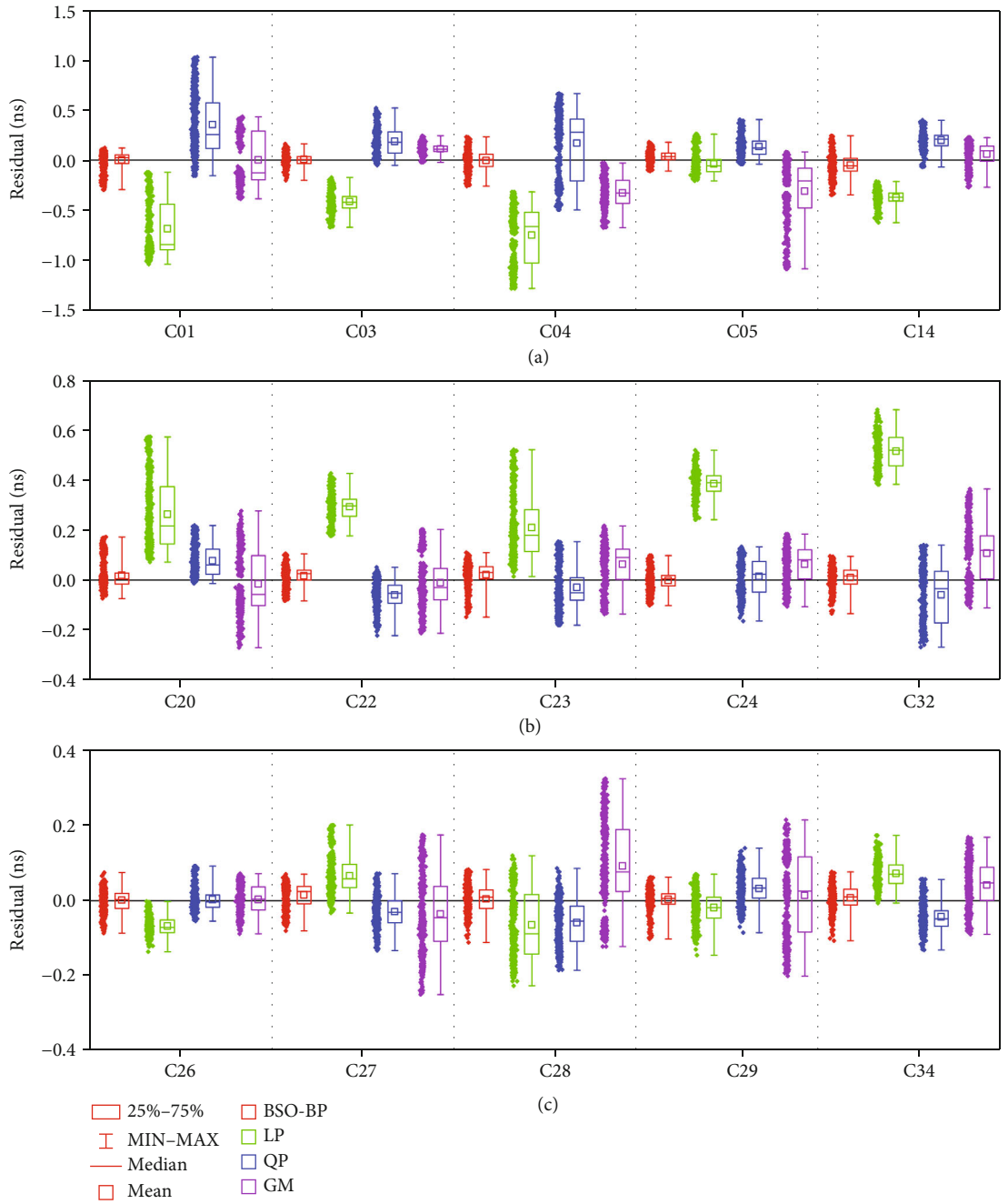

Figure 12: The statistics of 1-hour average STD of four models based on 6-hour SCB data: (a) residual distribution of five Rb clocks; (b) residual distribution of five Rb-II clocks; (c) residual distribution of five PHM clocks.

deteriorate gradually; however, the prediction stability of the QP model improves. It is noteworthy that the stability of the BSO-BP model is still the best, which improves by approximately 57.6%, 33.7%, and 64.2% as compared with the LP, QP, and GM models, respectively. Therefore, the proposed BSO-BP model has strong stability in the short-term clock bias prediction that does not change with the fitting time.

From the mean values of different atomic clocks, it is evident that the stability of PHM clocks is the best for different models, the stability of Rb-II clock is the second best, and the stability of the Rb clock is the worst. In addition, the stability of different atomic clocks does not change with the increase in fitting time, which is related to the material and physical properties of different atomic clocks. Therefore, the performance of the new generation BDS-3 satellite atomic clocks is greatly improved as compared with BDS-2.

3.6. Data Validation. To increase the convince of analysis, we use 6 consecutive days (DOY 164-169, 2020) of SCB data for accuracy and stability analysis. The first 6 hours and 12 hours of the daily SCB data are used to fit the predicted SCB of the next 1 hour, and the daily prediction accuracy

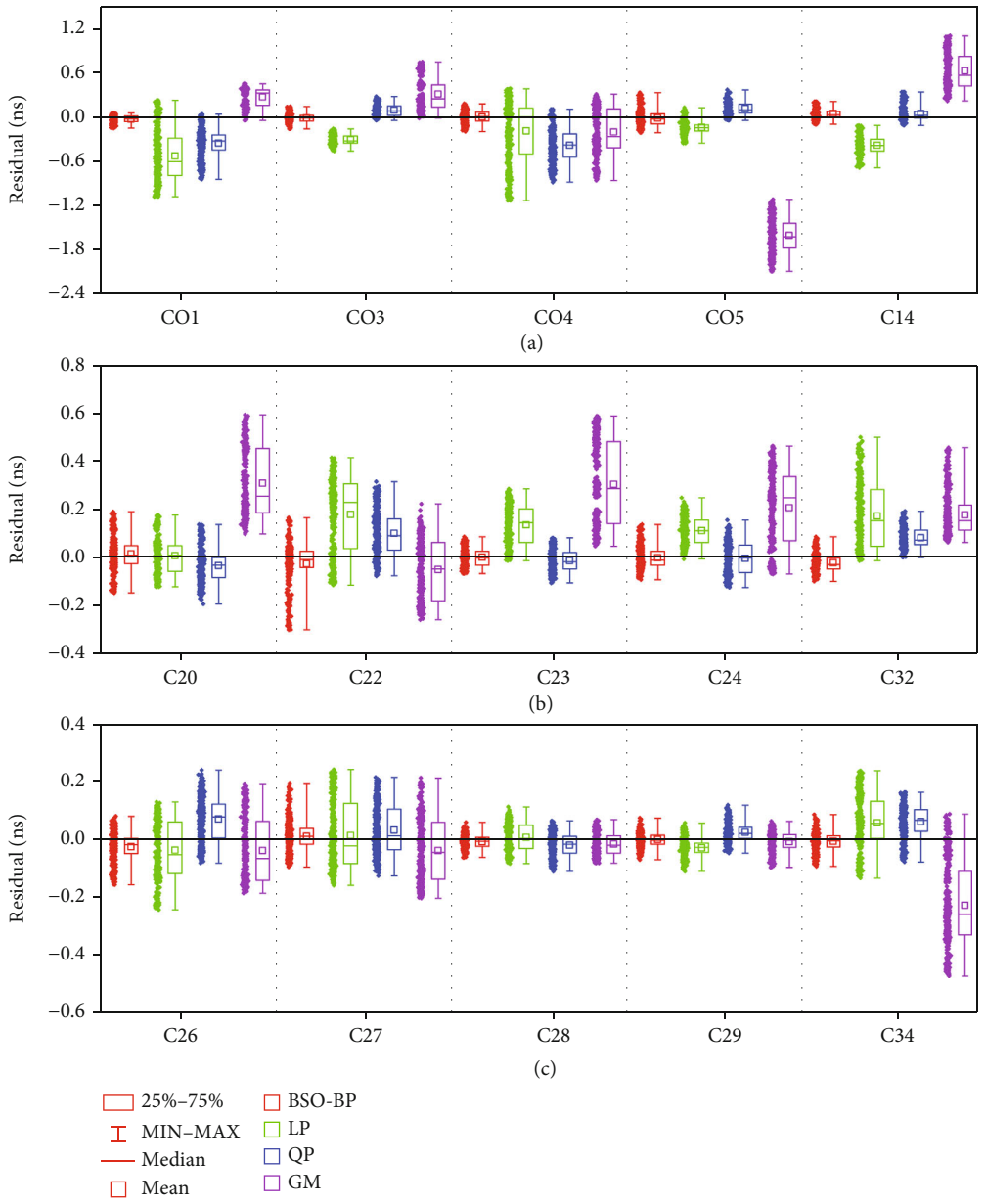

Figure 13: The statistics of 1-hour average STD of four models based on 12-hour SCB data: (a) residual distribution of five Rb clocks; (b) residual distribution of five Rb-II clocks; (c) residual distribution of five PHM clocks.

is counted to calculate the average value of the 6-day prediction accuracy. The results of prediction accuracy are shown in Figures 14 and 15.

It can be seen from Figures 14 and 15 that the BSO-BP model maintains the best prediction accuracy in the 6 consecutive days. At the same time, the four models have obvious differences in the prediction accuracy of different types of satellite clocks. The prediction accuracy of the PHM clock is the best, followed by the Rb-II clock, and the Rb clock is the worst. In general, the prediction accuracy value of the BSO-BP model for 6 consecutive days is very concentrated, which indicates that the model is not affected by SCB data of different dates. Tables 5 and 6, respectively, show the average prediction accuracy and stability of different clocks.

It can be seen from Table 5 that when fitting 6 hours and 12 hours to predict the next 1-hour clock bias, the prediction accuracy of the BSO-BP model improves by about 73.4%, 54.5%, and 54.3% and 72.6%, 43.4%, and 86% as compared with the LP, QP, and GM models, respectively. In addition, the prediction accuracies of PHM clock and Rb-II clock improved by more than 47%, as compared with that of the Rb clock. It can be seen from Table 6 that when fitting 6 hours and 12 hours to predict the next 1-hour clock bias, the prediction stability of the BSO-BP model improves by about 50.9%, 50.3%, and 42.4% and 55.2%, 36%, and 77.8% as compared with the LP, QP, and GM models, respectively. In addition, the prediction stability of PHM clock and Rb-II clock improved by more than 54%, as compared with that of

Table 4: The statistics of 1-hour average STD of four models based on 6-hour and 12-hour SCB data.

Clock type	6 h					12 h				
	LP	QP	GM	BSO-BP	Mean	LP	QP	GM	BSO-BP	Mean
Rb	0.166	0.185	0.169	0.076	0.149	0.202	0.125	0.221	0.071	0.155
Rb-II	0.086	0.077	0.102	0.045	0.077	0.097	0.061	0.135	0.054	0.087
PHM	0.047	0.041	0.085	0.031	0.051	0.078	0.056	0.087	0.036	0.064
Mean	0.100	0.101	0.118	0.050		0.125	0.080	0.148	0.053	

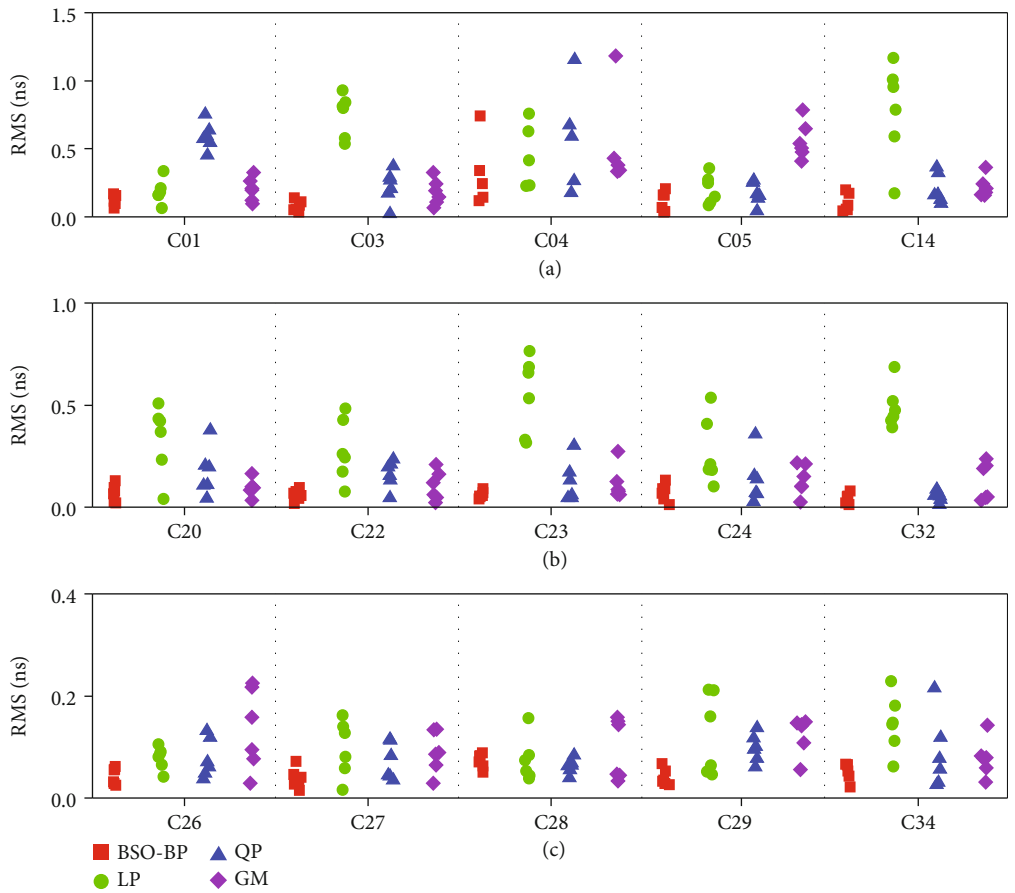

Figure 14: The prediction accuracy of 6 days for 1 hour using 6-hour SCB data: (a) residual distribution of five Rb clocks; (b) residual distribution of five Rb-II clocks; (c) residual distribution of five PHM clocks.

the Rb clock. This is consistent with the above analysis. Therefore, according to the 6-day analysis results, it can be seen that the prediction performance of the new-generation BDS-3 satellite atomic clock is greatly improved compared with that of the BDS-2.

4. PPP Validation with Predicted Clock

In order to verify the impact of the proposed clock model in static PPP, FHMJ and LEIJ of IGS stations are selected for the experiment. The processing strategies of static PPP are as follows: single BDS system is selected, without ionospheric combination; the parameter estimation adopts forward Kalman filtering. The observation file is downloaded from Crustal Dynamics Data Information System (CDDIS), and the sampling interval is 30 s. The orbit data adopts WUM precision orbit product. The DCB (Differential Code Biases) adopts the Chinese Academy of Sciences (CAS) product, and the antenna phase center adopts igs14_2186. The WUM precision clock data of the first 12 hours of the day (DOY 103, 2021) is used to predict the clock bias of next 1 hour. Predict SCB data is used for static PPP experiment. Static PPP was experimented with open source GAMP, and the residuals of every station in E (east), N (north), and U (up) directions can be calculated by comparing with the "reference values" which are published on the IGS website. Figures 16 and 17 are the static PPP positioning errors of FGMJ and LEIJ stations.

It can be seen from Figures 16 and 17 that the positioning errors of FFMJ and LEIJ stations can converge in static

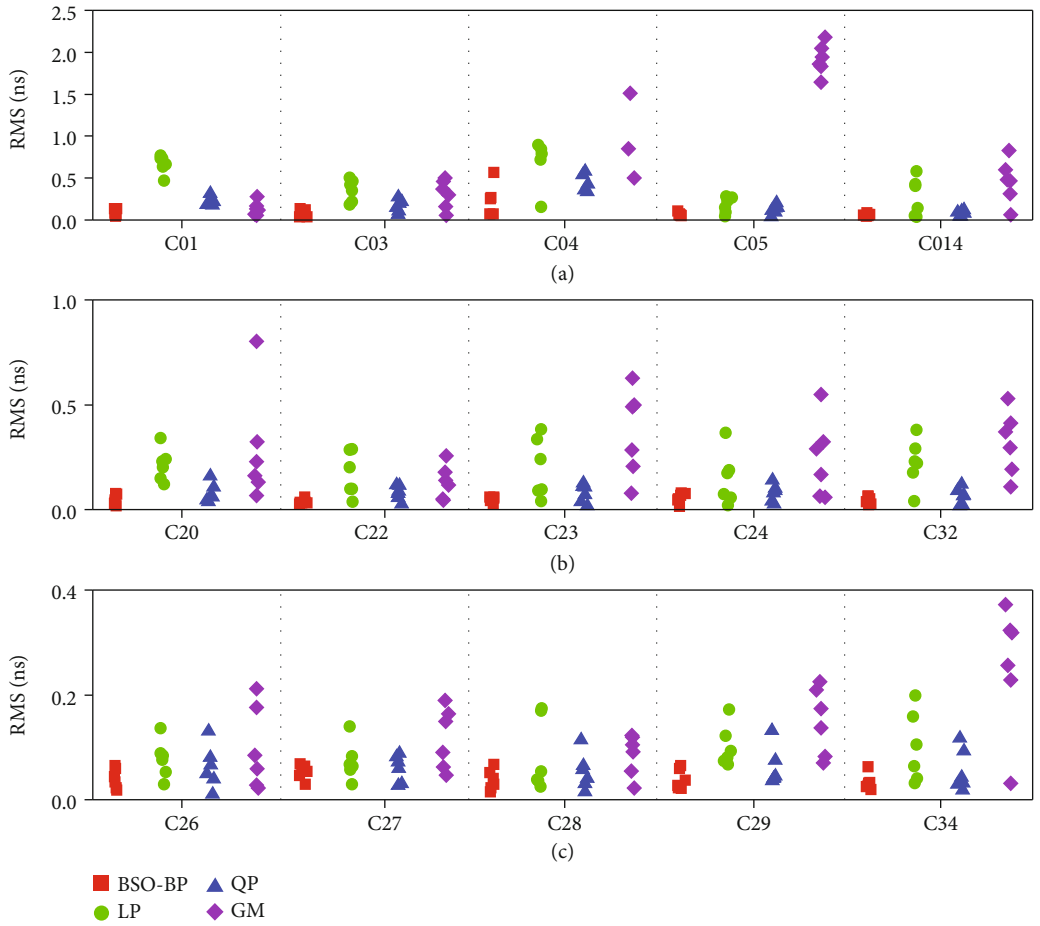

Figure 15: The prediction accuracy of 6 days for 1 hour using 12-hour SCB data: (a) residual distribution of five Rb clocks; (b) residual distribution of five Rb-II clocks; (c) residual distribution of five PHM clocks.

Table 5: The average prediction accuracy for 1 hour for three different types of clocks based on 6-hour and 12-hour SCB data.

Clock type	6 h					12 h				
	LP	QP	GM	BSO-BP	Mean	LP	QP	GM	BSO-BP	Mean
RB	0.473	0.352	0.339	0.145	0.327	0.428	0.205	0.964	0.107	0.426
RB-II	0.383	0.129	0.115	0.059	0.172	0.189	0.075	0.268	0.045	0.144
PHM	0.104	0.079	0.104	0.050	0.084	0.087	0.058	0.141	0.040	0.082
Mean	0.320	0.187	0.186	0.085		0.234	0.113	0.458	0.064	

Table 6: The average STD for 1 hour for three different types of clocks based on 6-hour and 12-hour SCB data.

Clock type	6 h					12 h				
	LP	QP	GM	BSO-BP	Mean	LP	QP	GM	BSO-BP	Mean
RB	0.253	0.266	0.197	0.154	0.218	0.192	0.153	0.567	0.104	0.254
RB-II	0.159	0.151	0.122	0.052	0.121	0.147	0.083	0.187	0.047	0.116
PHM	0.093	0.084	0.114	0.043	0.083	0.089	0.064	0.111	0.041	0.076
Mean	0.169	0.167	0.144	0.083		0.143	0.100	0.288	0.064	

PPP. In general, the convergence time of FFMJ station is about 40 epochs in E, N, and U directions, but the GM model is about 80 epochs in U direction. The convergence time of the LEIJ station is basically the same as those of the FFMJ station in E and N directions. But the convergence time in the U direction is slower which is achieved after 60 epochs. Therefore, the convergence time of the BSO-BP, LP, QP, and GM models is basically the same, while the convergence time of the E and N directions is better than that of the U direction. In addition, this paper conducts precision

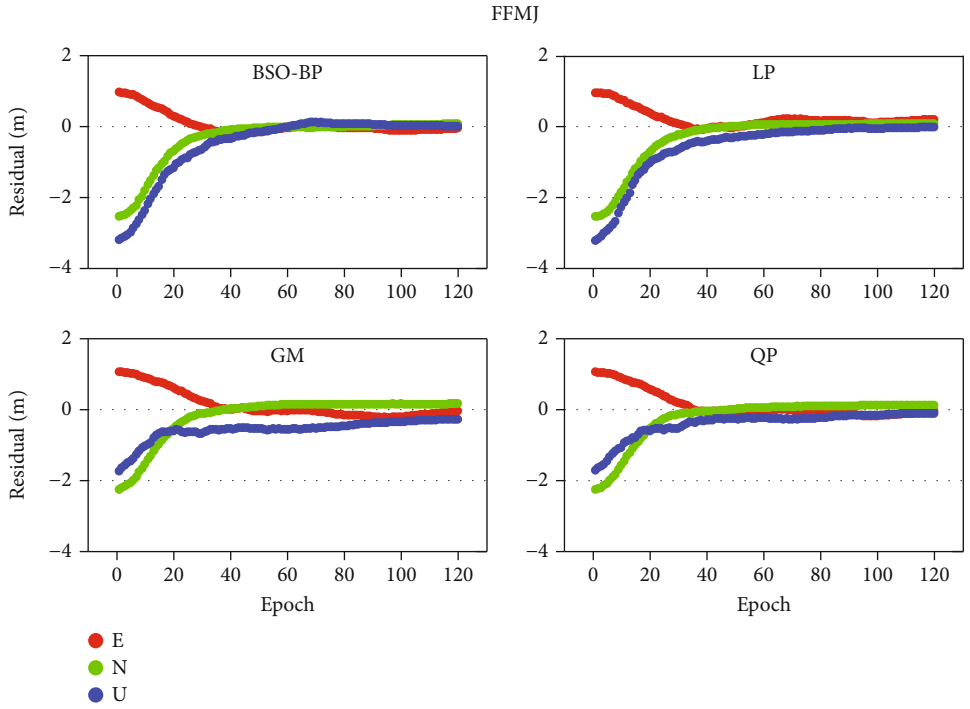

Figure 16: Residuals of the static PPP base on four clock model for FFMJ.

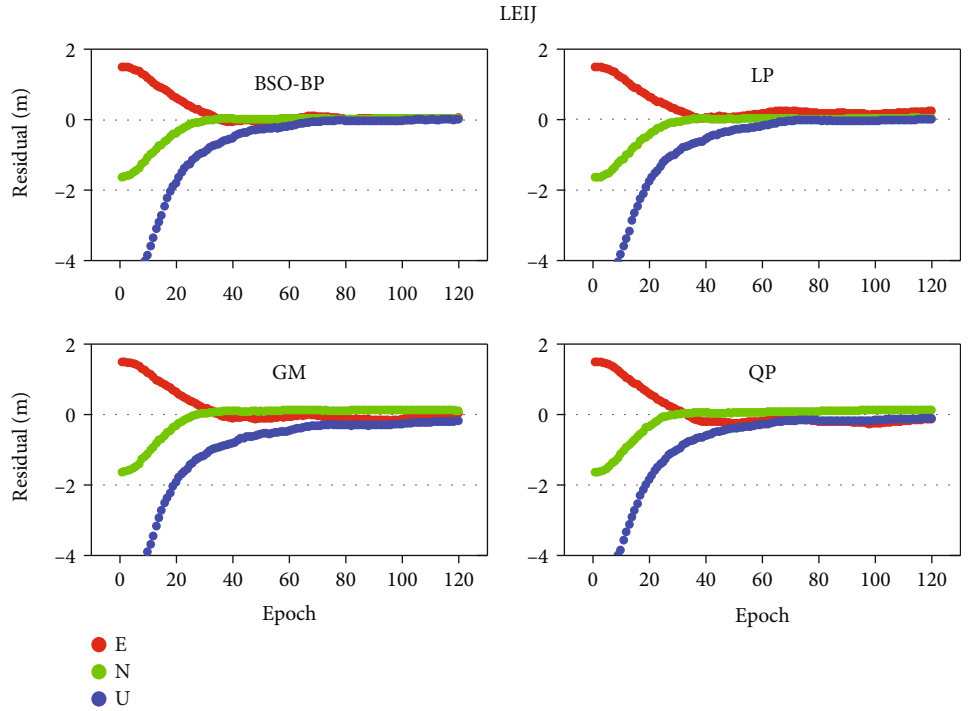

Figure 17: Residuals of the static PPP base on four clock model for FFMJ.

analysis on the positioning results of the four models, and the statistical results are presented in Table 7.

As can show in Table 7 that positioning accuracy of the BSO-BP model is basically within 5 cm in E, N, and U directions, while MMFJ station is 6.48 cm in E direction. Moreover, positioning accuracy of the LP model can reach 10 cm in the N and U directions, and positioning accuracy of the E direction can reach 20 cm, so positioning accuracy of the LP model is poor in E direction. Positioning accuracy of the QP model can reach 10 cm in the N directions, and

Table 7: The positioning accuracy statistics of static PPP.

Station	MMFJ				LEIJ			
Model	BSO-BP	LP	QP	GM	BSO-BP	LP	QP	GM
E	0.0648	0.1202	0.0900	0.1012	0.0335	0.1557	0.1960	0.0922
N	0.0378	0.0497	0.0807	0.1202	0.0185	0.0219	0.0729	0.0980
U	0.0392	0.0527	0.1478	0.3654	0.0364	0.0382	0.1656	0.3018

positioning accuracy of the E and U directions can reach 20 cm. In addition, positioning accuracy of the GM model is the worst that it can reach 20 cm in E and N directions, and the U direction can reach 36.54 cm.

Depending on the above analysis, we can know that the positioning accuracy of the BSO-BP model is better than the LP, QP, and GM models. In general, the LP model is preferable to the QP model, and the GM model is the worst. In the E direction, the positioning accuracy of the BSO-BP model improves by approximately 64.4%, 21.4%, and 16.8% as compared with the LP, QP, and GM models, respectively. In the N direction, the positioning accuracy of the BSO-BP model improves by approximately 65.6%, 63.3%, and 75.9% as compared with the LP, QP, and GM models, respectively. In the U direction, the positioning accuracy of the BSO-BP model improves by approximately 49.2%, 74.2%, and 88.7% as compared with the LP, QP, and GM models, respectively. Therefore, the positioning accuracy of the BSO-BP model can reach the centimeter level in E, N, and U directions, and the E and N directions are greatly improved for the LP, QP, and GM models.

5. Conclusions

Considering the simple structure and poor prediction accuracy of the traditional SCB prediction models, we present the BSO-BP model to predict the SCB. The prediction accuracy and stability of the model are further analyzed to evaluate the proposed method.

First, we observe that the frequency data is more suitable for performing predictions using the BP neural network. In addition, the BP model optimized by using the BSO performs better as compared to the original BP model.

Second, the prediction accuracy of the BSO-BP model gradually increases with an increase in fitting time. In addition, when using 6 hours and 12 hours data for predicting the next 1 hour, the prediction accuracy of the BSO-BP model improves by approximately 73.4%, 54.5%, and 54.3% and 72.6%, 43.4%, and 86% as compared with LP, QP, and GM models, respectively.

Third, when using 6-hour and 12-hour SCB data, the prediction stability of the proposed BSO-BP model improves by approximately 50.9%, 50.3%, and 42.4% and 55.2%, 36%, and 77.8% as compared with the LP, QP, and GM models, respectively.

Four, the analysis of different atomic clocks shows that the prediction accuracy of the PHM clock and Rb-II clock improved by more than 47%, as compared with the Rb clock. Moreover, the prediction stability also improves significantly as compared with the Rb clock. Therefore, the overall performance of the atomic clock based on BDS-3 is better than BDS-2.

Finally, the positioning accuracy of the BSO-BP model can reach the centimeter level in E, N, and U directions, and the E and N directions are greatly improved for the LP, QP, and GM models.

Data Availability

The experimental data in the manuscript are all public data and can be downloaded from the analysis center of Wuhan University website (http://www.igs.gnsswhu.cn/).

Conflicts of Interest

The authors declare that they have no conflicts of interest.

Acknowledgments

The authors would like to thank the Wuhan University for providing BDS-3 precise clock products. This work is supported by National Natural Science Foundation of China (No. 41704008), the Provincial Natural Science Foundation of Anhui (Nos. 2018085QD171 and 2018085MD130), the Open Research Fund of Coal Industry Engineering Research Center of Collaborative Monitoring of Mining Area's Environment and Disasters (No. KSXTJC202006), the introduction of talent research start-up fund of Anhui University of Science and Technology (No. 13200385), and the Key Project of Natural Science Research in Universities of Anhui Province (KJ2021A0443).

References

[1] X. Xu, X. Wang, J. Liu, and Q. Zhao, "Characteristics of BD3 global service satellites: POD, open service signal and atomic clock performance," *Romete Sensing*, vol. 11, no. 13, p. 1559, 2019.

[2] L. He, H. Zhou, Z. Liu, Y. Wen, and X. He, "Improving clock prediction algorithm for BDS-2/3 satellites based on LS-SVM method," *Romete Sensing*, vol. 11, no. 21, p. 2554, 2019.

[3] Y. Yang, Y. Xu, J. Li, and C. Yang, "Progress and performance evaluation of BeiDou global navigation satellite system: data analysis based on BDS-3 demonstration system," *Science China Earth Sciences*, vol. 61, no. 5, pp. 614–624, 2018.

[4] Y. Yu, M. Huang, G. Wang, R. Hu, and T. Duan, "A new BDS-2 satellite clock bias prediction algorithm with an improved exponential smoothing method," *Applied Sciences*, vol. 10, no. 21, p. 7459, 2020.

[5] T. Hadas, F. Teferle, K. Kazmierski, P. Hordyniec, and J. Bosy, "Optimum stochastic modeling for GNSS tropospheric delay estimation in real-time," *GPS Solutions*, vol. 21, no. 3, pp. 1069–1081, 2017.

[6] A. Cernigliaro and I. Sesia, "INRIM tool for satellite clock characterization: frequency drift estimation and removal," *Mapan*, vol. 27, no. 1, pp. 41–48, 2012.

[7] S. Ken, K. Paul, and R. Jim, "Developing an IGS time scale," *IEEE Transactions on Ultrasonics, Ferroelectrics, and Frequency Control*, vol. 50, no. 6, pp. 585–593, 2003.

[8] Z. Guo, P. Sun, and Z. Li, "Research on the improved algorithm of clock bias short-term prediction based on GM(1,1)+AR model," *Journal of Geodesy and Geodynamics*, vol. 40, no. 9, pp. 907–912, 2020.

[9] H. Song, S. Dong, L. Qu, X. Wang, and W. Guang, "Research on clock difference prediction using adaptive Kalman filter based on sage window," *Journal of Geodesy and Geodynamics*, vol. 38, no. 7, pp. 1809–1816, 2017.

[10] G. Huang, Q. Zhang, and G. Xu, "Real-time clock offset prediction with an improved model," *GPS Solutions*, vol. 18, no. 1, pp. 95–104, 2014.

[11] B. Cheng, X. Qiu, L. Ji et al., "Modeling and application of BDS satellite clock error," *Science of Surveying and Mapping*, vol. 44, no. 10, pp. 14–20, 2019.

[12] G. Wang, L. Liu, A. Xu, X. Su, and X. Liang, "The application of radial basis function neural network in the GPS satellite clock bias prediction," *Acta Geodaetica et Cartographica Sinica*, vol. 43, no. 8, pp. 803–817, 2014.

[13] X. Wang, H. Chai, and C. Wang, "TS fuzzy neural network to predict satellite clock bias," *Acta Geodaetica et Cartographica Sinica*, vol. 49, no. 5, pp. 580–588, 2020.

[14] Y. Wang, Z. Lv, Z. Chen, and Y. Cui, "Research on the algorithm of wavelet neural network to predict satellite clock bias," *Acta Geodaetica et Cartographica Sinica*, vol. 42, no. 3, pp. 323–330, 2013.

[15] X. Wang, H. Chai, C. Wang, and Y. Chong, "A wavelet neural network for optimal wavelet function to predict GPS satellite clock bias," *Acta Geodaetica et Cartographica Sinica*, vol. 49, no. 8, pp. 983–992, 2020.

[16] Y. Wang, Z. Lv, Y. Cui, H. Lv, and L. Li, "Predicting navigation satellite clock bias using a genetic wavelet neural network," *Geomatics and Information Science of Wuhan University*, vol. 39, no. 7, pp. 809–814, 2014.

[17] L. Lan, C. Ren, Y. Liang, and F. Li, "Prediction of satellite clock bias based on wavelet decomposition and genetic wavelet neural network," *Journal of Guilin University of Technology*, vol. 37, no. 1, pp. 125–130, 2017.

[18] Z. Zhao, F. Yang, Z. Zhang, and L. Zhang, "Satellite clock error prediction based on gray neural network optimized by particle swarm algorithm," *Journal of Navigation and Positioning*, vol. 6, no. 2, pp. 53–81, 2018.

[19] W. Li, S. Bian, Q. Ren, C. Mei, and X. Pan, "Kernel extreme learning machine based on particle swarm optimization for prediction of Beidou uItra-rapid clock offset," *Journal of Astronautics*, vol. 40, no. 9, pp. 1080–1088, 2019.

[20] G. Xiao, J. Ou, G. Liu, and H. Zhang, "Construction of a regional precise tropospheric delay model based on improved BP neural network," *Chinese Journal of Geophysics*, vol. 61, no. 8, pp. 3139–3148, 2018.

[21] K. Bo, N. Hoang, X. Bui, H. Bui, and N. Trung, "Prediction of the sorption efficiency of heavy metal onto biochar using a robust combination of fuzzy C-means clustering and back-propagation neural network," *Journal of Environmental Management*, vol. 293, article 112808, 2021.

[22] B. Islam, Z. Baharudin, and P. Nallagownden, "Development of chaotically improved meta-heuristics and modified BP neural network-based model for electrical energy demand prediction in smart grid," *Neural Computing and Applications*, vol. 28, no. 1, pp. 877–891, 2017.

[23] M. Panda, S. Nandi, and P. Sarkar, "A comparative study of performance of different back-propagation neural network methods for prediction of resonant frequency of a slot-loaded double-layer frequency-selective surface," *Indian Journal of Physics*, vol. 89, no. 12, pp. 1283–1286, 2015.

[24] Q. Liang, H. Han, X. Cui, H. Qing, and Y. Fan, "Comparative study of probabilistic neural network and back propagation network for fault diagnosis of refrigeration systems," *Science and Technology for the Built Environment*, vol. 24, no. 4, pp. 448–457, 2018.

[25] X. Zhou, R. Urayama, T. Uchimoto et al., "Application of back-propagation neural networks to defect characterization using eddy current testing," *International Journal of Applied Electromagnetics and Mechanics*, vol. 64, no. 1-4, pp. 817–825, 2020.

[26] J. Song, W. Song, Y. Gao, and P. Sun, "Hydrogen atomic clock difference prediction based on improved back propagation neural network," *Chinese Journal of Scientific Instrument*, vol. 37, no. 2, pp. 454–460, 2016.

[27] G. Huang, B. Cui, Q. Zhang, W. Fu, P. Li, and Y. Lin, "Real-time clock offset prediction model with periodic and neural network corrections," *Journal of Astronautics*, vol. 39, no. 1, pp. 83–88, 2018.

[28] D. Lu, J. Ou, and S. Yu, "Prediction of the satellite clock bias based on MEA-BP neural network," *Acta Geodaetica et Cartographica Sinica*, vol. 49, no. 8, pp. 993–1003, 2020.

[29] T. Wang, Y. Long, and L. Qiang, "Beetle swarm optimization algorithm: theory and application," *Univerzitet u Nišu*, vol. 34, no. 15, pp. 5121–5137, 2020.

[30] P. Singh, A. Kaur, R. Batth, S. Kaur, and G. Gianini, "Multi-disease big data analysis using beetle swarm optimization and an adaptive neuro-fuzzy inference system," *Neural Computing and Applications*, vol. 33, no. 16, pp. 10403–10414, 2021.

[31] L. Wang, Q. Wu, F. Lin, S. Li, and D. Chen, "A new trajectory-planning beetle swarm optimization algorithm for trajectory planning of robot manipulators," *IEEE Access*, vol. 7, pp. 154331–154345, 2019.

[32] Y. Mu, B. Li, D. An, and Y. Wei, "Three-dimensional route planning based on the beetle swarm optimization algorithm," *IEEE Access*, vol. 7, pp. 117804–117813, 2019.

[33] L. Wang and X. Bi, "Risk assessment of knowledge fusion in an innovation ecosystem based on a GA- BP neural network," *Cognitive Systems Research*, vol. 66, no. 46, pp. 201–210, 2021.

[34] Y. Liu, "The development and forword problems of neural network theory," *Information and Control*, vol. 1, pp. 31–46, 1999.

[35] C. Feng and S. Hu, "Kinematic inverse solution of mechanical arm based on improved beetle antennae search," *Engineering Journal of Wuhan University*, vol. 53, no. 12, pp. 1121–1128, 2020.

[36] S. Xu, S. Zhou, and D. Pi, "Damage identification of high-piled wharf's lateral bent structure based on quantum beetle swarm

optimization algorithm," *Port & Waterway Engineering*, vol. 8, pp. 97–99, 2020.

[37] B. Hariharan, R. Siva, S. Kaliraj, and P. Prakash, "ABSO: an energy-efficient multi-objective VM consolidation using adaptive beetle swarm optimization on cloud environment," *Journal of Ambient Intelligence and Humanized Computing*, vol. 12, no. 4, pp. 4303-4304, 2021.

[38] Y. Wang, Z. Lv, Z. Chen, L. Huang, and L. Li, "A new data preprocessing method for satellite clock bias and its application in WNN to predict medium-term and long-term clock," *Geomatics and Information Science of Wuhan University*, vol. 41, no. 3, pp. 373–379, 2016.